Scaled versus real-scale tests

Identifying scale and model errors in wave damping through woody vegetation

Kalloe, Su A.; Hofland, Bas; Van Wesenbeeck, Bregje K.

DOI
10.1016/j.ecoleng.2024.107241

Publication date
2024

Document Version
Final published version

Published in
Ecological Engineering

Ecological Engineering 202 (2024) 107241

Contents lists available at ScienceDirect

Ecological Engineering

journal homepage: www.elsevier.com/locate/ecoleng

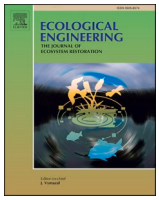

Scaled versus real-scale tests: Identifying scale and model errors in wave damping through woody vegetation

Su A. Kalloe [a,*], Bas Hofland [a], Bregje K. Van Wesenbeeck [a,b]

[a] Delft University of Technology, Stevinweg 1, Delft 2600 GA, Zuid-Holland, the Netherlands
[b] Deltares, Boussinesqweg 1, Delft 2629 HV, Zuid-Holland, the Netherlands

ARTICLE INFO

Keywords:
Scaled model
3D-printed tree mimics
Wave attenuation
Pollard willow trees

ABSTRACT

Vegetation in front of levees, dikes and seawalls can decrease wave energy and therefore contribute to the safety against flooding. However, wave damping predictions by vegetation are still inaccurate due to measurement and modelling uncertainties. Many studies focused on finding reliable predictive tools using scaled flume tests with vegetation mimics. Scaling down vegetation can however lead to discrepancies with realistic scales, known as scale errors. In this work scaled tests were conducted on 3D-printed elastic replicas of willow trees and compared with real-scale experiments. We identified differences in measured wave dissipation between the scaled hydraulic model (1:10) and its real-scale prototype with 5 m high live willow trees under storm conditions (1:1). The maximum measured wave damping (30%) was roughly 1.5 times higher than the real-scale experiments (20%). Following the same trend of the real-scale experiments, this amount of wave height damping declined for larger water levels. Largest effects are argued to be due to increased viscous damping (smaller branch Reynolds numbers) and non-exact flexibility scaling. These significant deviations illustrate that full-scale experiments, although expensive, are still needed to validate the results of scaled experiments for woody vegetation. Alternatively, accounting for these discrepancies can make scaled experiments more reliable and expensive real-scale experiments less needed for wave damping studies on woody vegetation.

1. Introduction

Nature-based flood defences, specifically vegetation in front of dikes, can increase the safety against flooding while providing many other ecosystem services (such as storing carbon, sheltering habitat, and trapping sediment) (Riis et al., 2020). Over the last decades these solutions are increasing in popularity in the face of climate change (IPCC, 2022). Nonetheless, implementation of these solutions maintains a challenge as design guidelines are missing. One of the reasons is that many wave damping predictions are based on data from scaled flume tests or field experiments that cover only mild wave conditions. Validation of these predictions is still scarce, leading to uncertainties in the design of these hybrid flood defences (Vuik, 2019). To correct for scale errors in scaled experiments, we need validation under storm conditions especially in comparison with similar scaled tests.

There are few measurements covering extreme hydraulic conditions at large-scale (e.g., Möller et al. (2014)) and in the field (e.g, Vuik (2019)). However, the link between realistic scale and scaled tests is missing. Measuring extreme conditions during field campaigns is difficult as these events do not occur often, are not in a controlled and repeatable setting, and pose difficulties with measuring equipment. As a result, most field campaigns are during mild wave climate (such as Phuoc and Massel (2006); Quartel et al. (2007); Bao (2011); Norris et al. (2017)) and only few studies cover extreme weather (such as Infantes et al. (2012); Vuik (2019)), mainly on sea-grasses and salt marshes. Large-scale testing facilities with controlled conditions can be used to test vegetation-wave interactions on realistic scales. However, conducting full-scale (scale 1:1) and large-scale (i.e., up to 1:4 scale (National Research Council (U.S.), 1999)) experiments are relatively costly and time consuming, making experiments at reduced scales with vegetation mimics attractive. Hence, scaled flume experiments have been frequently conducted in the past to investigate wave propagation through live grassy vegetation (Ozeren et al., 2014; Maza et al., 2015) or with mimics representing woody vegetation, such as mangroves (Ismail et al., 2012; Hu et al., 2014; Maza et al., 2019). However, down-scaling experiments can lead to discrepancies with findings at full scale. Deviations between scaled models and their prototype can generally be contributed to three main sources: model effects, measurement effects,

* Corresponding author.
E-mail address: s.a.kalloe@tudelft.nl (S.A. Kalloe).

https://doi.org/10.1016/j.ecoleng.2024.107241
Received 14 November 2023; Received in revised form 15 February 2024; Accepted 24 March 2024
Available online 1 April 2024

and scale effects (Heller, 2011). Firstly, model effects occur when prototype features cannot be captured well enough in a modelling facility, such as material properties and boundary conditions. Secondly, specific characteristics of a measuring technique may result in measurement effects. Thirdly, relevant *force-ratios* between the prototype and its scaled model may deviate, which can lead to scale effects. Differences in the formulation of vortices is one example of these scale effects. These deviations are likely to resonate in numerical models with inherent errors.

In this manuscript, we compare wave damping results from scaled tests with real-scale tests to obtain insight in possible scaling errors in scaled flume tests. For this, we use real-scale experiments with woody vegetation, specifically live willow trees (van Wesenbeeck et al., 2022), to design the set-up of scaled experiments with 3D-printed trees. The latter scaled experiments (scale 1:10) mimic the full-scale experiments in terms of hydraulic conditions, location of the equipment, and consider the geometry and flexibility of the trees. With the results, a first assessment of possible correction for wave damping through woody vegetation when using scaled tests is made. This will make scaled experiments more reliable and may lessen the need for expensive large-scale experiments in the future. Most importantly, current wave-predictions can be made more reliable with knowledge on these scale errors.

2. Methods

2.1. Experimental setup

The prototype tests were conducted in a 291 × 5 × 9.5 (l × w × h) m^3 wave flume, of which 200 m of the total length was used for the experiments. A detailed description of these tests can be found in van Wesenbeeck et al. (2022). We used a 1:10 scale model ($n_L = 10$); this was the largest scaled model that could fit in the available flume (i.e., l × w × h = 40 × 0.8 × 1 m^3). A segment of this wave flume was used for these tests to replicate the geometry of the prototype section. For this, a divider made of wood was used to reduce the width of the flume to 0.5 m and a dike construction was built with two slightly different slopes (namely, a composite 1:3.6 upper and 1:3 lower slope) mimicking the dike slopes of the real-scale tests. This dike was placed such that the desired flume length of 20 m was obtained. The scaled experimental set-up is shown in Fig. 1. The wave gauges (WG1–10) and one video camera from the side of the flume (camera 1: *SONY Handycam* 25 *fps*) were mainly used for analysis in this manuscript.

2.2. Scaling

Scale errors increase with scale factor (n_l), which is the ratio between the characteristic length in real-world scale (L_p) and in model scale (L_m) (Heller, 2011). To avoid scale effects, scaled models require the following similarities with their prototype: geometric similarity, kinematic similarity, and dynamic similarity (Hughes, 1993). For dynamic similarity, the most relevant ratios controlling the investigated phenomenon should be selected and ideally kept constant to the prototype values.

For models of free-surface flows Froude similarity, is typically used, ensuring that most wave-related phenomena are well reproduced, calculated as follows $Fr = \frac{U}{\sqrt{(gh)}}$ with the velocity (U), gravitational constant (g), and the water depth (h). The Reynolds number ($Re = \frac{UD}{\nu}$, where ν is the kinematic viscosity of the fluid and D is a representative diameter), which represents the ratio of inertial force to viscous force, is typically reduced at smaller scale. If *Re* is larger than a certain threshold, forces that flow around objects separate and the forces on these objects (governed by inertial pressures) will generally follow Froude scaling (Heller, 2017). The tested hydrodynamic conditions were therefore scaled following *Fr* similitude.

If the motion of (branches of) vegetation is important, the Cauchy number also becomes important (Luhar and Nepf, 2016; Cavallaro et al., 2018; van Veelen et al., 2020). This is related to the elastic force, with Cauchy being a reliable representative number:

$$Ca = \frac{\rho_w U^2 D l^3}{EI},$$

where ρ_w = density of water; U= velocity; D = representative diameter

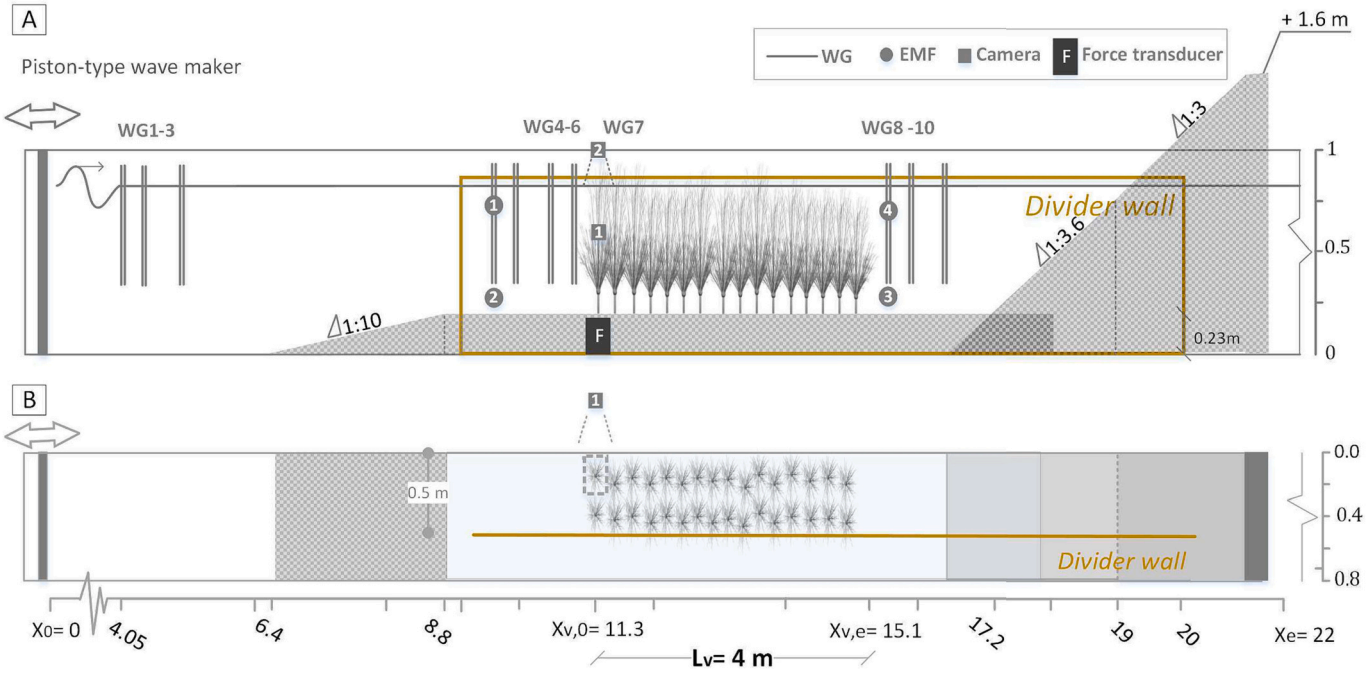

Fig. 1. The set-up of the 1:10 scaled tests (A) shows a side-view of the set-up, where the wave gauges (WG), electromagnetic flow meters (EMF), two cameras, and force transducer (F) are shown along the flume; (B) shows a top view of the set-up, where the two rows of the trees and the divider wall can be seen. The geometry of real-scale test setup was 10 times larger.

of the object; l = object's length; E = Young's modulus; I = second moment of area. We scaled flexibility using the Cauchy number, implying that the material of the branches is chosen such that the Young's modulus of the model, E_m, equals $1/10$ ($1/n_l$) times the Young's modulus of the prototype, E_p. The E_p was assumed to be within a range of 3800–4500 (Armanini et al., 2005). We selected a material within this range, namely Soft-Flexible PLA, with a Young's modulus of 390 MPa.

Scaling based on *Fr* automatically leads to the correct scaling of certain non-dimensional numbers such as the Keulegan-carpenter number ($KC = \frac{UT}{D}$, representing the ratio of drag-to-inertia force (Keulegan and Carpenter, 1958)). However, other relevant ratios may deviate from prototype scale, such as the Reynolds number (*Re*) as we considered *Fr* similitude and kept the fluid identical between the model and prototype.

2.3. Design of tree mimics

We focused on vegetation tests excluding the leaves, as leaves were found to have an insignificant effect ($\leq$ 4%) on the amount of wave damping while having a relatively large frontal-surface area compared to the branches (van Wesenbeeck et al., 2022). The tests included represent two vegetation configurations, namely: trees with 100% canopy density, and 50% canopy density (i.e., where 50% of the branches of each tree were removed).

Tree mimics were made considering a 1:10 geometric scale of the real size trees and including surface areas for different branch orders taken from Kalloe et al. (2022a). The primary branches, which are the main branches that sprout from the tree knot, were categorized into three classes based on manual measurements of the diameter at the knot (i.e., base diameter, D_B). The canopy from the tree simulations in Kalloe et al. (2022a) consisted of these three branch classes, namely: class 1 ($Db \geq 50$ mm), class 2 ($20 < D_B \leq 50$ mm), and class 3 ($D_B \leq 20$ mm). Furthermore, these classes are built-up from branch orders, starting at the tip of the branches (order 1, smallest branch) until the primary branch is reached at the knot (order 3). Fig. 2 shows an example of three different branch classes; the simplified branches; and finally an impression of the entire tree including one red colored medium branch (class 2), which was used to follow its movement. With the 3D printer the minimum diameter that could be printed was 1 mm, while the smallest order branches had a diameter of 0.3 mm. Hence, we decided to have less smallest order branches to still achieve a frontal-surface area distribution over the vertical, which was similar to the live trees (see Fig. 3). However, geometric deviations between the two scales are inevitable using mimics. For more details on how these mimics were build, we refer to Kalloe et al. (2022b).

2.4. Forest characteristics

The trees were placed in two rows of 16 trees each; an identical configuration to the real-scale experiments. Canopy densities and their distribution over the flume were kept largely the same as in the real-scale experiment. Each individual tree was generated with the same number of main branches of the three classes, while the exact configuration of the branch was randomly generated from allometric relations based on a real pollard willow tree (see Fig. 2). The entire tree was 3D-printed. The trunk and knot needed to be stiff, while the branches of the canopy were printed with flexible material (see Section 2.2). For attaching the trees to the bed, a streamlined disk of 5 mm thickness was added to the lower part of the trunk. Fig. 4 shows the live forest and printed mimics. The live branches that sprout from the knot's circumference have a slight curve. As the modelled branches were not curved as in reality, the divergence angle is somewhat smaller leading to a higher density in the center compared to the live canopies. This is not expected to influence the wave damping as the inter-branch distance is still large.

2.5. Experimental conditions

The hydrodynamic conditions and relevant dimensionless numbers (i.e, $\widetilde{Re}$, $\widetilde{KC}$ and $\widetilde{Ca}$) are compared at both scales in Table 1. This table shows the values for the largest branches (*class*1 *order*3), and the smallest branches (*order*1).

Calculating the non-dimensional numbers (such as *Re* and *KC*) is not straightforward as a tree consists of different components with distinct characteristics (such as diameters and Young's modulus) and are subject to a varying velocities. The trees were therefore separated into components, such as a knot, trunk, and different order branches. The non-dimensional numbers were determined for layers over the water column for these separate components. Fig. 4 shows an example of how Re_i is calculated for a live pollard willow tree. This method shows that the main branches (order 3) of each class (class 1, 2 and 3) were divided into layers over the water depth because of the change in diameter and velocity values over the vertical axis. The diameter tapering of the main branches sprouting from the knot (order 3) was assumed to be linear over the height. For this a minimum diameter (i.e., order 1 or tip of the branch) of 3 mm for the live tree and 1 mm for the printed tree was assumed, while the base diameters of the branches (D_b) were similar

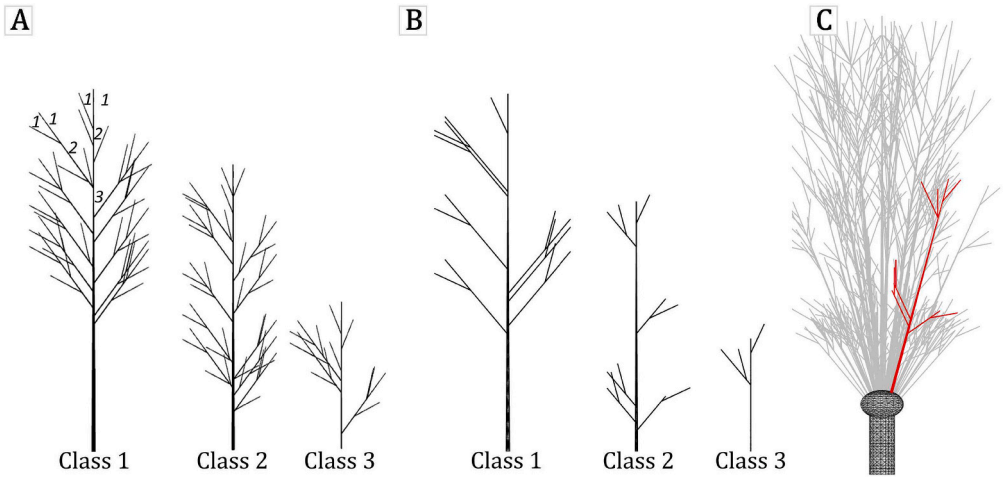

Fig. 2. (A) A 2D example of the 3 branch classes used to create a tree model of the live trees; and an example of how a branch (i.e., class 1) is built-up from different branch orders (order 1, 2, and 3), (B) simplified branch classes for the 3D-printed mimics, (C) example of an entire tree, where one medium branch was colored (red) for tracking the branch motion. (For interpretation of the references to color in this figure legend, the reader is referred to the web version of this article.)

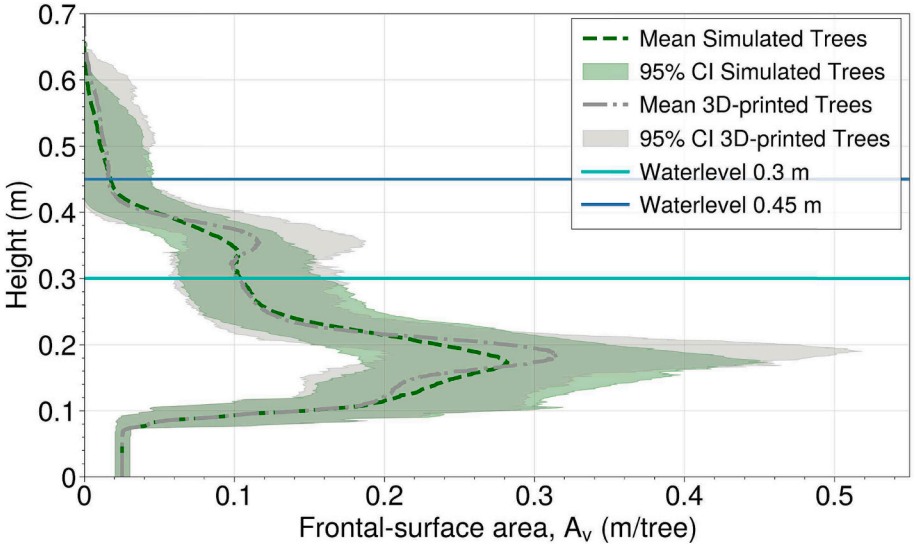

Fig. 3. The calculated frontal-surface area profiles of the simulated (Kalloe et al., 2022b) and 3D-printed trees with the two tested water levels indicated, namely 0.3 and 0.45 m.

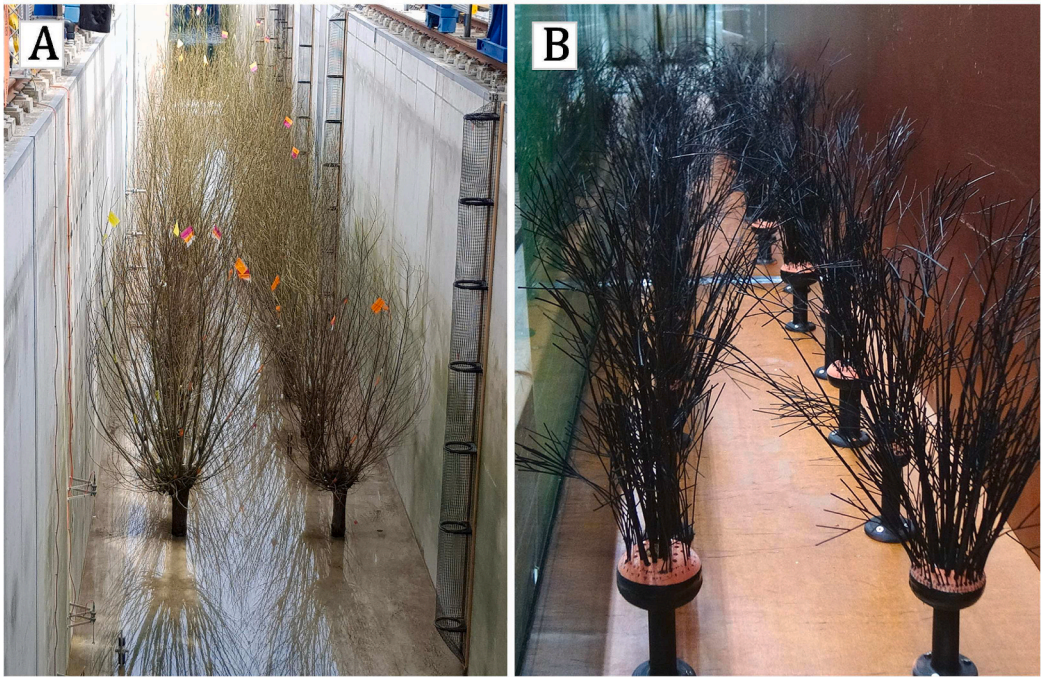

Fig. 4. (A) The real-scale experiments with the 50% density live trees, (B) the scaled experiments with 50% density 3D-printed trees (1:10 scale).

between the live tree and printed tree. This also implies that the tapering (branch slope) of the live trees is larger than the tapering of the branch mimics.

$$\widetilde{Re} = \frac{1}{N}\sum_{i=1}^{N}\frac{(\overline{u}_h(z).\overline{D}(z))}{\nu} \quad (1)$$

$$\widetilde{KC} = \frac{1}{N}\sum_{i=1}^{N}\frac{(\overline{u}_h(z).T_p)}{\overline{D}(z)} \quad (2)$$

$$\widetilde{Ca} = \frac{\rho I^3 \overline{u}_h(z)^2 \overline{D}(z)}{E\overline{I}(z)} \quad (3)$$

$$I = \frac{\pi \overline{D}(z)^4}{64} \quad (4)$$

The horizontal velocity distribution, $u_h(z)$, was calculated with linear wave theory, using H_s and T_p, as follows:

$$u_h(z) = \omega_p \frac{H_s}{2}\frac{cosh(k_p z)}{sinh(k_p h)},$$

where wave angular frequency $\omega_p = \frac{2\pi}{T_p}$; wave number $k_p = \frac{2\pi}{L_p}$; and the wave length $L_p = \frac{gT_p^2}{2\pi} tanh(k_p h_f)$. Finally, the average value was calculated over the water column. The $\widetilde{KC}$ value was calculated in this similar manner. This method was different for $\widetilde{Ca}$, we used the average diameter

Table 1
An overview of the wave parameters (i.e., water depth at the forest h_f, significant wave height H_s, and peak wave period T_p) and dimensionless parameters (i.e., $\widetilde{Re}$, $\widetilde{KC}$ and $\widetilde{Ca}$) for the largest (Class1 Order3, base diameter = 62 mm) and smallest branches (Order 1, diameter = 3 mm) of the real-scale (R001-R006) and scaled experiments (S001-S006).

	Test	h_f (*m*)	H_s (*m*)	T_p (*s*)	$\widetilde{Re}_{large} \times 10^3(-)$	$\widetilde{Re}_{small} \times 10^3(-)$	$\widetilde{KC}_{large}(-)$	$\widetilde{KC}_{small}(-)$	$\widetilde{Ca}_{large}(-)$	$\widetilde{Ca}_{small}(-)$
Real scale	R001	3	0.50	2.83	20.2	1.2	22	372	0.09	0.059
	R002	3	1.17	3.58	50.3	2.9	68	1160	0.59	0.345
	R003	3	0.50	4.00	21.9	1.3	32	563	0.11	0.065
	R004	3	1.01	5.66	46.2	2.6	96	1665	0.52	0.280
	R005	4.5	1.61	4.90	46.5	3.2	132	1767	4.28	0.425
	R006	4.5	1.52	6.93	46.8	3.2	181	2475	4.28	0.412
1:10 Scale	S001	0.3	0.05	0.9	0.7	0.1	21	112	0.09	0.0002
	S002	0.3	0.12	1.13	1.6	0.3	66	347	0.56	0.009
	S003	0.3	0.05	1.26	0.7	0.1	32	168	0.11	0.0002
	S004	0.3	0.10	1.79	1.5	0.3	94	499	0.49	0.008
	S005	0.45	0.16	1.55	1.6	0.3	122	530	3.51	0.011
	S006	0.45	0.15	2.19	1.6	0.3	169	742	3.51	0.011

and average velocity over the height of each tree component (l).

2.6. Wave damping, transmission and reflection

The incoming waves travel from deep water (measured by WG1–3) to the foreshore step (measured by WG4–5), where shoaling and depth-induced breaking of waves can occur. These waves travel further through the synthetic forest, where the incoming wave height decreases due to wave damping by the forest; and the transmitted waves reflect back by the dike slope behind the forest. The incident wave heights were determined at deep water (WG1–3), in front of the forest (WG4–6), and in front of the dike (WG8–10), using the method of Mansard and Funke (1980) for 3 wage gauges. For the real-scale experiments the wave separation was done considering a combination of measurements, namely: using the same method with 3 wave gauges in deep water; and co-located wave height and velocity gauges on the platform in front and behind the willow forest using an adapted Maximum Entropy Method (van Wesenbeeck et al., 2022).

The amount of wave damping (Dr) was afterwards calculated in the same manner as used in van Wesenbeeck et al. (2022):

$$Dr = \frac{H_{m0_{cal}} - H_{m0_{wil}}}{H_{m0_{cal}}}, \tag{5}$$

where H_{m0} is the incident wave height behind the forest (i.e., in front of the dike measured by WG8, WG9 or WG10).

2.7. Branch deflection

The branch deflection at both scales was analysed due to variations in dimensionless numbers, as shown in Table 1. This can impact the motion and, hence, impact the wave damping. We focused on a medium branch (i.e., *Class* 2) situated in the first row of the forest, facing the wave-maker. The motion of the live branch was estimated by observing an orange colored flag attached on the tip of the branch, while the mimicked branch of interest was well captured from the side of the flume (see Section 2.1) and tracked by its distinct color (i.e., white) compared to the color of the canopy (i.e., black). The flag was captured with cameras above the flume (see Appendix B, Fig. B.1A) with the camera locations obtained from photos of the camera setup. A grid with known dimensions (see Appendix B, Fig. B.1B) was used to approximate the "real" deflection of the flag, and hence, the live branch. Furthermore, we used *Premiere Pro 2022* to remove lens distortions associated to our type of camera (*GoPro HERO4*).

First, the distance between the flag and the camera was approximated to find the required corrections; then the deflections were obtained. The uncertainty bandwidth of the data is found by a sensitivity analysis on the relative distances. We refer to Appendix B for the detailed description of the procedure.

Finally, the deflection is related to a certain wave height in front of the tree. We used linear wave theory to translate the surface elevations at WG6 to a location near the tree. For the scaled tests this was not needed, as the wave gauge just in front of the forest (WG7) could be used.

The qualitative analysis for obtaining the branch motion is performed on one test of 3 *m* water depth (R201) as the class 2 branch (medium) was not clearly visible during the high water level tests, h_f = 4.5 m (i.e., R205 and R206).

2.8. Extending data set

Besides the scaled tests that were equivalent to the real-scale tests (shown in Table 1), additional scaled tests were conducted. These scaled tests were performed with 100% density mimics and included additional wave conditions for the nearly submerged case (i.e., $h_f = 0.45\ m$); and tests under fully submerged conditions (i.e., $h_f = 0.57\ m$). The entire test overview is shown in Table A.1. These additional tests, thus far, lack the validation of the real-scale experiments. Their results are therefore corrected to obtain the wave damping by live willow trees under these additional hydrodynamic conditions. This was achieved by applying a correction factor (f_n) to the measured wave damping at small-scale. This factor is defined as the average ratio of the measured wave damping between the two scales, considering the 100% canopy density tests.

3. Results

3.1. Comparing wave damping

Two vegetation configurations, namely 100% canopy density and 50% canopy density, were tested at real-scale and 1:10 scale under hydrodynamic conditions shown in Table 1. Wave damping measured during the scaled experiments is compared to wave damping of the real-scale experiments, as shown in Fig. 6. Data from the scaled experiments are all positioned above the grey solid line (real-scale tests); hence, measured wave damping by synthetic willows at a 1:10 scale was overall larger than wave damping by realistic willow trees.

3.2. Comparing branch motion

The deflection of one medium branch was determined using video images from both scaled and real-scale experiments. The obtained estimated deflections are shown in Fig. 7. The data points shown in this figure represent single waves taken from one irregular wave test with ca. 1000 waves at real-scale (R201 with h_f = 3 m, H_s = 0.5 m, T_p = 2.83 s) and its equivalent scaled test (S201 with h_f = 0.3 m, H_s = 0.05 m, T_p = 0.9 s). The uncertainty bandwidth for live branches is added as the exact positions of the live branch and camera were unknown. Overall,

deflections of mimicked branches were lower than the observed deflections of the live branches. For both scales, a positive trend between wave height and deflection is seen.

3.3. Correcting wave damping

The amount of wave damping through the forest with 100% canopy density is shown for emergent, nearly submerged, and fully submerged conditions (see Fig. 8). Only the emergent and nearly submerged cases have equivalent real-scale results, while the fully submerged tests are shown with and without a correction factor, $f_n = 0.5$. After applying the correction factor, the results show that the fully submerged trees dampen significantly less waves than the emergent and nearly submerged cases.

4. Discussion

Until now, many studies on wave damping through woody vegetation have used data from scaled experiments that are susceptible to scale errors; which in turn can result in discrepancies in wave attenuation through real-scale forests. Here, we confirm and illustrate, the mismatch in wave damping between scaled and full-scale tests. Wave damping by a pollard willow forest is over-predicted by approximately a factor 1.5 in 1:10 scaled tests. This can be caused by multiple factors that we elaborate on below.

First, Froude similarity is applied for scaling these type of experiments, however, simultaneously the Reynolds number will deviate (i.e., relatively lower) from its prototype value. Usually a lower limit for Reynolds is used to still get similar wake formation behind the vegetation elements, yet very little to no data of full-scale tests with extreme conditions exists with live vegetation, thus the validation is lacking (e.g., Wu and Cox (2015); Maza et al. (2019)). In this study, we used data from full-scale experiments with live willow trees to design 1:10 scaled experiments, following Froude similitude. We scaled the trees according to the Cauchy number to replicate similar motion. However, there is no common approach to calculate these non-dimensional numbers (e.g., Fr, Re, and Ca). Most research uses a single value for defining dimensionless numbers. This is fitting for vegetation with relatively simple geometry such as salt marsh (e.g., Luhar and Nepf (2016); Jacobsen et al. (2019)). However, it becomes less representative for woody vegetation that consists of a trunk and canopy, which consists of branches of different orders. Previous studies on mangroves tried to include this by defining dimensionless numbers for roots, the stem and the canopy, (e.g., Maza et al. (2019); He et al. (2019); Kelty et al. (2022)). This approach assumes an idealized vegetation model, implying that the elements of the roots or canopy did not vary in size or properties (e.g., single diameter).

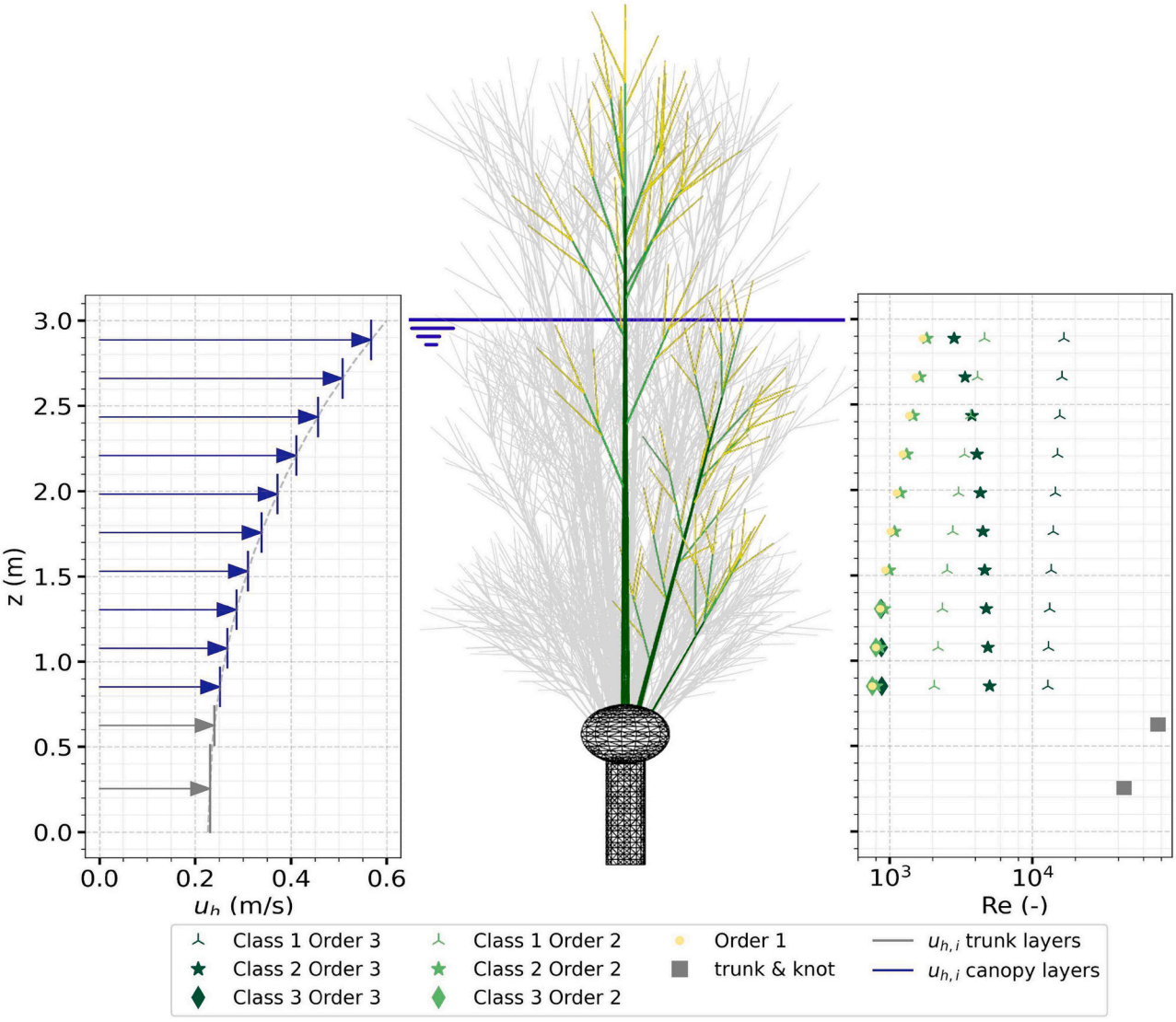

Fig. 5. Example of how the Reynolds number is calculated for test R001.

In the current study, we calculated dimensionless discrete numbers for the various components of the tree (i.e., trunk and various branch orders) in the water column and showed that this results in a wide range of values for the dimensionless numbers (see Fig. 5). Dimensionless numbers were defined at the scale of the single elements. Other studies (e.g., Maza et al. (2019); He et al. (2019)) may used other characteristic length scales based on total canopy width or summed branch diameters, which can result in higher Reynolds numbers.

Second, the frontal-surface area distribution along the height of each individual trees, which was shown to be an important parameters in previous studies, was determined using various methods described in (Kalloe et al. (2022a)). During these experiments a comprehensive representation of the trees was discussed and we used these results for 3D-printing the mimics; hence, we regarded the frontal-surface area to be well-represented. Furthermore, fluid forces are argued to be more prominent in scaled experiments than in the prototype. This has been referred to in previous work as 'damping' effect (e.g., Heller (2011)). Hence, calibration runs (tests without vegetation) were included in our test program to account for the influence of bed and wall friction at both scales. At the same time, we excluded the leaves from the scaled tests as large over-estimations of wave damping are expected, as Cauchy scaling of leaves and finding the appropriate material is prohibitively challenging. Most importantly, the leaves of the real scale willows had an insignificant effect on the wave damping under storm conditions van Wesenbeeck et al. (2022). In the end, we observed still overestimation effects in the scaled tests that could not be fully explained by a single reason. It is assumed that this large component can be caused by the following reasons: (1) dissimilar Reynolds number leading to increased viscous damping, (2) simplified flexibility scaling, and (3) other mechanisms (such as air entrainment differences).

4.1. Reynolds scale effects

Firstly, *Fr* similitude was used to scale the global hydrodynamic conditions of these experiments and *Ca* for the trees, while *Re* was not considered. *Re* is nevertheless important to ensure similar wake formation behind the structure, making both *Fr* and *Re* necessary for investigating the wave transformation through vegetation. Generally lower

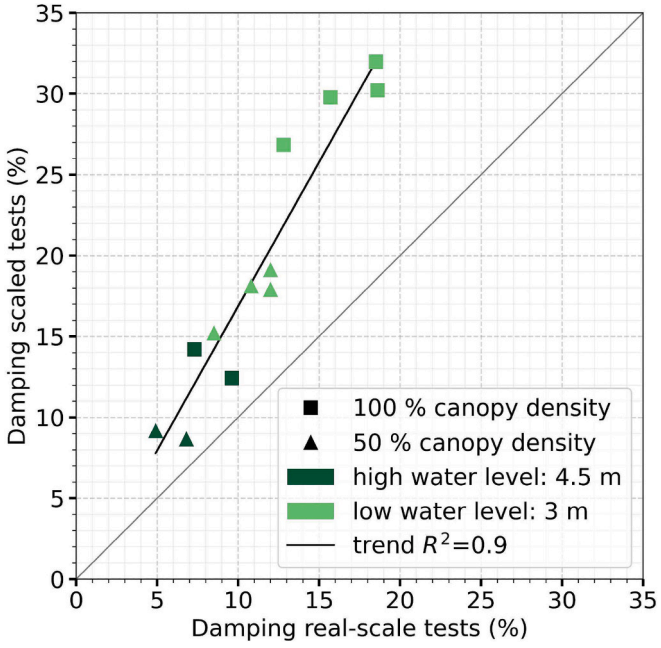

Fig. 6. Measured wave damping from real-scale experiments versus measured wave damping from scaled experiments (grey line); for vegetation with 100% canopy density (squares) and 50% density (triangles).

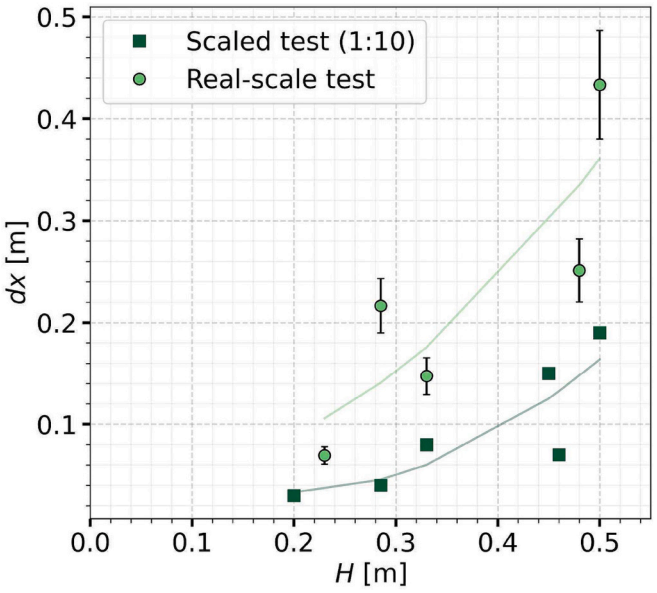

Fig. 7. shows the maximum deflection (*dx*) with corresponding wave height (*H*). These results are for one test of the full-scale tests, R201 (squares) and scaled tests, S201 (circles). The deflection and wave height of test S201 were multiplied by $n_L = 10$.

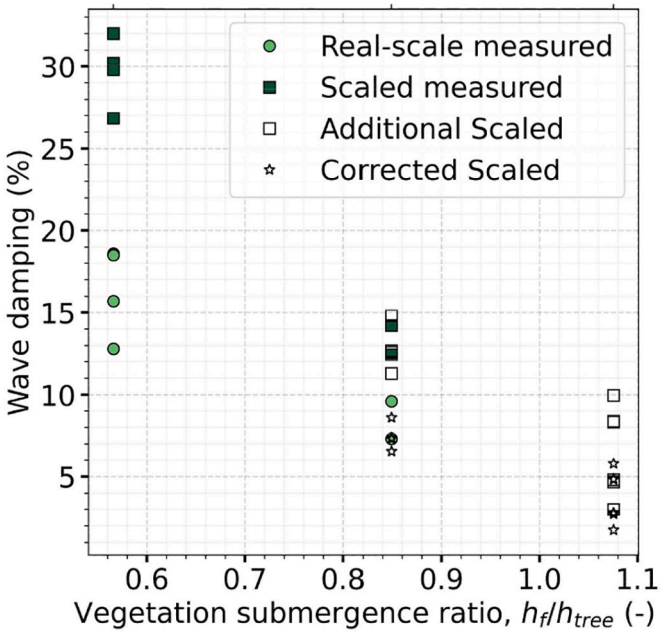

Fig. 8. shows the measured wave damping through 100% density trees at real-sale (green circles) and scaled (green squares) for different submergence ratios; and additional scaled tests (squares) and the expected damping (stars) after applying a correction for scale errors on these additional scaled tests.

Reynolds numbers were obtained during these scaled experiments, compared to the real-scale tests that were in fully turbulent flow. As a consequence of this, higher drag forces can be expected for lower Reynolds numbers. The *Re*-C_D relation is represented in Fig. 9 for a single rigid cylinder in flow Sumer and Fredsoe (1998). The $\widetilde{Re}$ range of the largest and smallest branches were added to this figure, illustrating the difference in regimes between the two tested scales, especially for the smallest diameter branches. This difference alone could lead to an increase of 5% points in wave damping through the 40-m-long willow

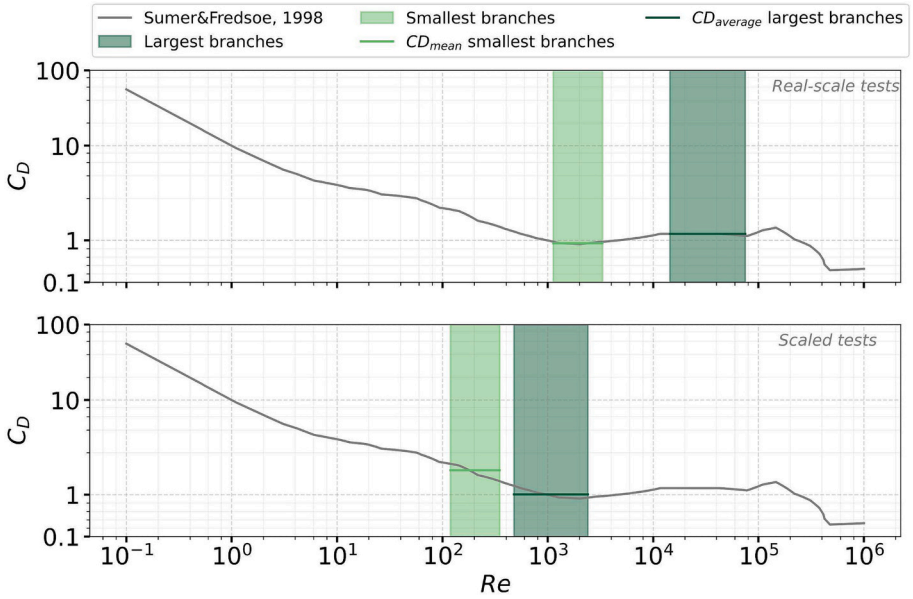

Fig. 9. Shows the *Re* range of the real-scale tests (upper) and the scaled tests (below) for the smallest and largest branches.

forest. This estimation was based on the conventional analytical formula (Dalrymple et al. (1984); Mendez and Losada (2004)), using a weighted average drag coefficient (C_{Dw}) based on Fig. 9 for both the average live tree ($C_{Dw} \approx 1$) and the mimicked tree ($C_{Dw} \approx 1.37$) (see Appendix C).

For high Reynolds numbers ($\geq 10^4$), which usually is the case in real-scale settings, the friction drag only accounted for maximum 2% of the total drag force and pressure drag is the main contributor (Achenbach, 1968). For lower Reynolds numbers, where there is not yet complete turbulent wake development behind the branches, the skin friction might increase depending on the relative roughness of the object (Moody Diagram). This is also expected between 3D-printed branches and fluid, leading to higher friction and causally higher wave damping. On the other hand, the roughness of parts of the live tree can lead to earlier transition to turbulence (drag crisis). As this is mainly the case for the trunk and knot of the willow trees, this most likely has a negligible effect on the measured wave damping.

The orientation of the cylinder (branch) relative to the incoming velocity can also affect the forces if the angle of attack is larger than 35° (Sumer and Fredsoe, 1998). Moreover, this dependency disappears for oscillatory flow when KC is large enough ($KC \geq 20$) (Sumer and Fredsoe, 1998). The angle of the side branches relative to the trunk (0°) can be 30° for the 2*nd* order branches and can reach up to 55° for the 1*st* order branches (i.e., smallest branches), leading to angle of attack $\approx 35^{\circ}$ for the smallest branches and the tests have a minimum KC of 22, which is yet within both previously mentioned ranges, hence well-resembled.

4.2. Flexibility model effects

Secondly, woody vegetation also moved when subjected to storm waves, as discussed in van Wesenbeeck et al. (2022). For simplicity, vegetation is usually considered to behave as rigid cylinders (e.g., Hu et al. (2014); Tinoco and Coco (2018); Sonnenwald et al. (2019)). However, these simplifications can lead to wave damping over-estimations. Vegetation motion was shown to impact the amount of wave damping van Veelen et al. (2020). Relatively smaller deflection was measured in the scaled model compared to the real-scale tests, which can be a consequence of the variability of the Young's Modulus. Studies showed that the *E*-modulus of branches is not constant across different sections of the branches, such as Starrenburg et al. (2023), while we used a single value for the Young's modulus, *E*. For example, Sutili et al. (2010) conducted bending tests for 6 different diameter classes of *Salix* × *Rubens* (willow species), and showed that the average Young's modulus ranged from ≈ 3.000–5000 N/mm^2 depending on the diameter class.

Besides simplifications regarding the Young's modulus, we also simplified the geometry. Branches with a smaller diameter than 1 *mm* were not possible with the 3D-printer. To still get similar frontal surface area, we lumped the smallest order branches together. The volume is however not similar between model and prototype. This could result in deviations in inertia forcing; however, we do not expect inertia to play an important role relative to the drag force as the KC number of these small branches is large (see Table 1), indicating drag-dominated regime (Sumer and Fredsoe, 1998).

The geometric simplifications lead to thicker and thereby also stiffer 1*st order* branches than required, and stiffer objects are generally known to dampen more than flexible alternatives (Mullarney and Henderson, 2010). One could argue that this is also the case for the printed branches. The flag used for the motion analysis at real-scale, was attached on a 1*st order* branch – a relatively more flexible branch than its scaled mimic. The analysis on the maximum deflection of the tip of the branch (see Fig. 7) illustrated that the live branches had larger tip displacement than the 3D-printed trees. This is in line with the wave damping measurements: less wave damping for the live trees (more flexible small branches) that also showed more deflection under waves. The discrepancies between the deflections at the two scales were more apparent for higher waves; and we expect a similar trend for the other tests. Unfortunately, this comparison could not be made for these irregular wave tests with larger significant wave heights or higher water levels, as the branch of interest was not visible during these tests. On the contrary, the contribution of the smallest branches to the wave damping is also unknown. We expect the motion of the tip of the branches (i.e., smallest diameter and highest flexibility) to have less impact on the wave damping than the motion of the primary branches. Previous work for example used an effective length parameter for blades (Lei and Nepf, 2021). It is therefore relevant to investigate the effectiveness of the different branch orders in wave damping.

4.3. Aeration (Weber) scale effects

Thirdly, waves that travel through the forest, undergo wave transformations and also changes in air entrainment (Tomiczek et al., 2020) that can impact the interaction with the structure, and in turn also the

wave damping results from scaled tests. Furthermore, only few studies compared scaled experiments to prototype tests for wave damping by woody vegetation. For example, Kelty et al. (2022) showed a good agreement between synthetic mangrove forests at two scales. These tests had relatively large scale and rigid tree models, such that here this aeration effect was isolated. The direct effect of decreased mass density does not influence wave damping, as mass density is present both in the wave energy flux and the dissipation term, such that it cancels out in the final dissipation equation, Appendix C.1. Overall this effect is deemed to be smaller than the first two effects.

5. Conclusions

Scaled tests with Cauchy-scaled pollard willow mimics (20%) resulted in higher wave damping compared to real-scale tests (30%). This over-prediction is argued to be mainly due to scale effects (Reynolds dissimilarity) and to model effects, impacting flexibility of the canopy. The trade-off between *Fr* and *Re* and flexibility modelling is challenging but nevertheless important to get reliable wave damping results from these tests. Concluding, real-scale studies on realistic vegetation are still warranted to improve our understanding of wave attenuation by flexible woody vegetation. The wave damping by trees is a multi-scale problem. The different elements of a tree (e.g., trunk and branches) are characterized by distinct dimensions and mechanical properties; the drag force experienced by the tree is influenced by the vortices and wave development at canopy-scale and element/branch-scale. We showed the importance of considering all elements of a tree (i.e., smallest to largest size branches) as this leads to a wider range of relevant force ratios. Capturing these elements at a smaller scale was technically and time-wise not feasible. To ensure proper up-scaling for flood risk estimations, correction factors can be considered as presented in this study. Still, more research is needed on varying the scale of the tests, the vegetation properties such as flexibility, and identifying other uncertainties. Based on our results, scaled experimental studies should only be used for conservative wave damping estimates, if no real-scale validation study is possible.

CRediT authorship contribution statement

Su A. Kalloe: Conceptualization, Formal analysis, Investigation, Methodology, Visualization, Writing – original draft. **Bas Hofland:** Conceptualization, Funding acquisition, Supervision, Writing – review & editing, Methodology, Project administration, Resources. **Bregje K. Van Wesenbeeck:** Conceptualization, Funding acquisition, Supervision, Writing – review & editing, Project administration, Resources.

Declaration of competing interest

The authors declare that they have no known competing financial interests or personal relationships that could have appeared to influence the work reported in this paper.

Data availability

Data will be made available on request.

Acknowledgments

This study is part of the research program WOODY. This project is financed by the Dutch Research Council (NWO) via the Open Technology Program, number 17194. We thank Oord, Boskalis, Rijkswaterstaat, World Wildlife Fund, Stowa, and VP Delta for their contributions to this research. We also acknowledge the support we received from everyone who helped building the vegetation mimics, especially King Shawn for 3D-printing all the components.

Appendix A. Experimental conditions

Table A.1
Overview of the entire scaled test program with equivalent real-scale tests.

Vegetation	Small-scale test	Real-scale test	h_0(m)	h_f(m)	H_{s0}(m)	T_p(s)
50% density	S101	R101	0.53	0.3	0.05	0.9
	S102	R102	0.53	0.3	0.117	1.13
	S103	R103	0.53	0.3	0.05	1.265
	S104	R104	0.53	0.3	0.101	1.79
	S105	–	0.68	0.45	0.05	0.9
	S106	–	0.68	0.45	0.103	1.265
	S107	–	0.68	0.45	0.05	1.265
	S108	–	0.68	0.45	0.1	1.79
	S109	R109	0.68	0.45	0.161	1.55
	S110	R110	0.68	0.45	0.152	2.19
100% density	S201	R201	0.53	0.3	0.05	0.9
	S202	R202	0.53	0.3	0.117	1.13
	S203	R203	0.53	0.3	0.05	1.265
	S204	R204	0.53	0.3	0.101	1.79
	S205	–	0.68	0.45	0.05	0.9
	S206	–	0.68	0.45	0.103	1.265
	S207	–	0.68	0.45	0.05	1.265
	S208	–	0.68	0.45	0.1	1.79
	S209	R209	0.68	0.45	0.161	1.55
	S210	R210	0.68	0.45	0.152	2.19
	S211	–	0.8	0.57	0.05	0.9
	S212	–	0.8	0.57	0.103	1.265
	S213	–	0.8	0.57	0.05	1.265
	S214	–	0.8	0.57	0.1	1.79
	S215	–	0.8	0.57	0.161	1.55
	S216	–	0.8	0.57	0.152	2.19
No Vegetation	S001	R001	0.53	0.3	0.05	0.9
	S002	R002	0.53	0.3	0.117	1.13
	S003	R003	0.53	0.3	0.05	1.265

(*continued on next page*)

Table A.1 (*continued*)

Vegetation	Small-scale test	Real-scale test	h_0(m)	h_f(m)	H_{s0}(m)	T_p(s)
	S004	R004	0.53	0.3	0.101	1.79
	S005	–	0.68	0.45	0.05	0.9
	S006	–	0.68	0.45	0.103	1.265
	S007	–	0.68	0.45	0.05	1.265
	S008	–	0.68	0.45	0.1	1.79
	S009	R009	0.68	0.45	0.161	1.55
	S010	R010	0.68	0.45	0.152	2.19
	S011	–	0.8	0.57	0.05	0.9
	S012	–	0.8	0.57	0.103	1.265
	S013	–	0.8	0.57	0.05	1.265
	S014	–	0.8	0.57	0.1	1.79
	S015	–	0.8	0.57	0.161	1.55
	S016	–	0.8	0.57	0.152	2.19

Appendix B. Branch motion real-scale experiments

The camera set-up of the real-scale tests is shown in Fig. B.1. Every 0.5 m along the wall was horizontally marked (with dots and crosses), while the vertical was marked every 1.25 m with the black cross and half-way with a red dot (62.5 cm).

The maximum tip deflection of a class 2 primary branch ($20 \leq D_b \leq 50\ mm$) on the tree in the first row of the forest was determined. The total length of the branch was approximated using $D_b - branchlength$ relations from Fig. 8 in Kalloe et al. (2022a), where it was shown that the total length can be between 2 and 4 m. We chose the average total length to be 3 m.

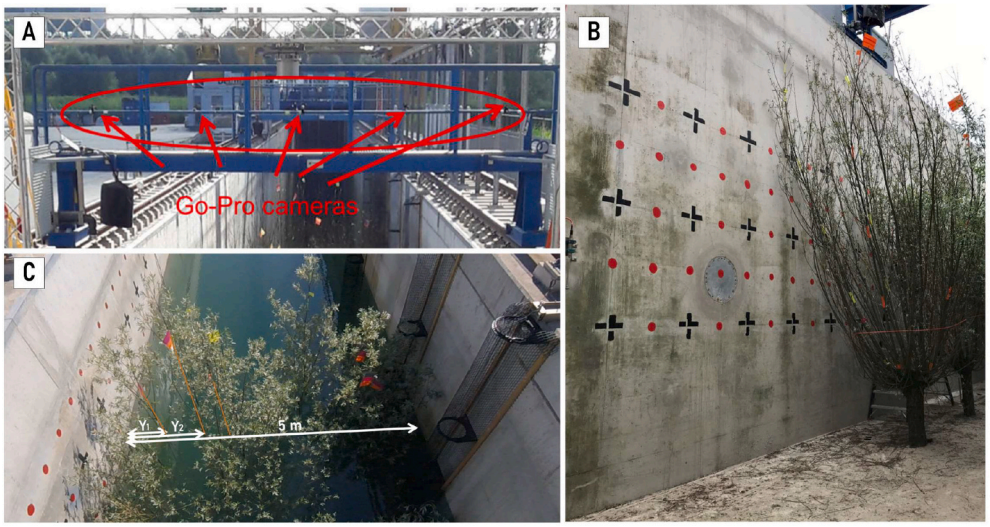

Fig. B.1. Set-up of the cameras for the qualitative analysis of branch motion from the real-scale experiments.

First, the wave signal measured at WG6 (x = 96.5 m) was translated to the position in front of the tree (x = 113.5 m). We validated this by applying this translation to the measurements by RADAC01 and predicted the measurements at WG6. This is shown is Fig. B.2 for test R201.

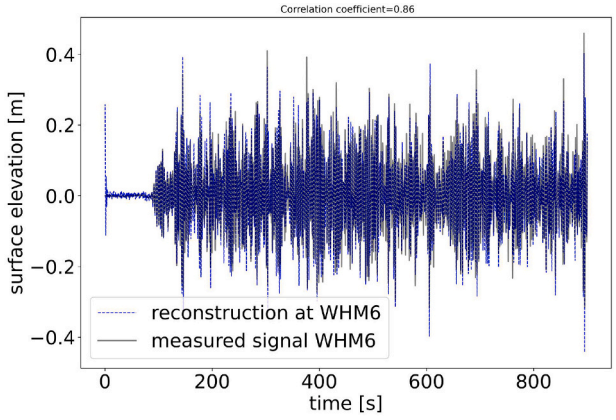

Fig. B.2. Measured elevation signal versus the reconstruction at that location of the signal for R201.

After this, we selected 5 wave heights (Table B.1) to approximate the maximum branch deflection. These wave heights were chosen such that the

flag was still visible during the wave attack.

Table B.1
The selected wave heights for obtaining maximum branch deflections.

R201		*S201*	
H (m)	frame	H (m)	frame
0.23	484	0.020	3440
0.29	2037	0.029	2947
0.33	1306	0.033	366
0.48	1508	0.046	4593
0.50	1677	0.050	4395

B.1. Sensitivity analysis

The deflection of the live branches was determined by video analysis. This was a qualitative analysis were the maximum deflection related to a certain wave height could only be approximated as the exact position of the camera and the flag relative to the reference object were unknown. A sensitivity analysis was performed to visualize the range of expected outcomes. The following ranges in values were considered:

length of the branch, $l_{br} = 3 \pm 1$ m,

- distance flag from wall, $dy_{w-flag} = 0.64 \pm 0.2$ m and $dz_{w-flag} = 0.5 \pm 0.2$ m, and
- the relative distance of the camera to the flag: $dx_c = 4 \pm 1$ m; $dy_c = 3.11 \pm 1$ m $dz_c = 5.69 \pm 1$ m.

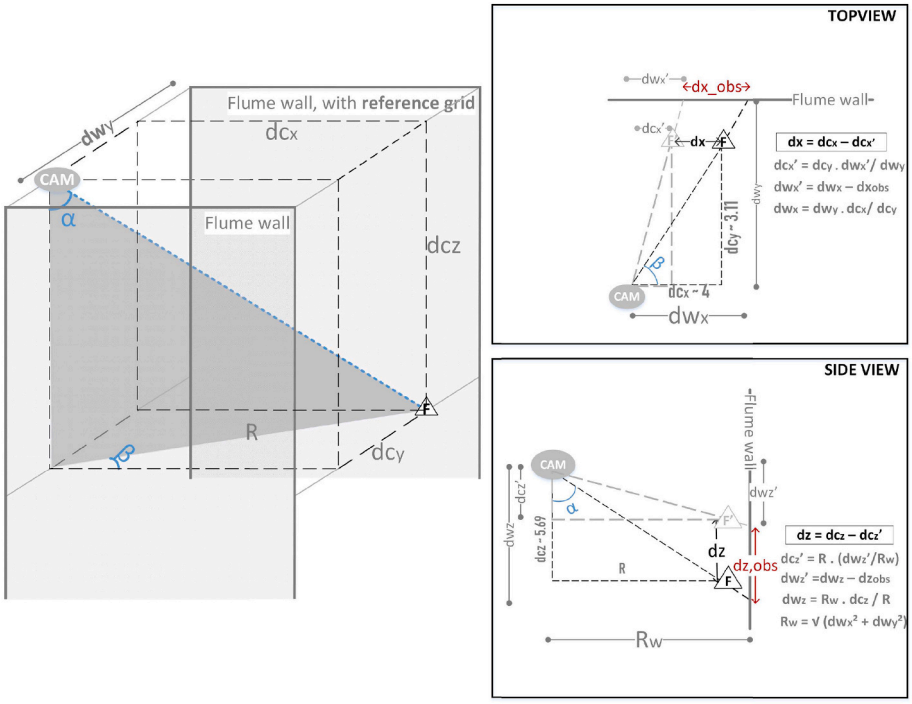

Fig. B.3. The correction applied in x-direction following the flag on the *class* 2, medium branch.

Appendix C. Difference in Wave damping by *Re*

The aim of this section is to get an indication of how much of the measured overestimation of wave damping could be assigned to the Reynolds differences of the different branches. Firstly, the average drag coefficient was determined for the smallest and the largest branches. These values are based on Fig. 9, showing the C_D-*Re* relation for a smooth rigid cylinder.

Table C.1
Average values from Reynolds-CD graph of a smooth cylinder.

$C_{D,average}$	Real-scale tests	Scaled tests
Largest branches (order 3)	1.15	1
Smallest branches (order 1)	0.93	1.58

Afterwards, the weighted average drag coefficient of the canopy was calculated, where the weight is assigned to the ratio of the total frontal area. Tables C.2 and C.3 show the weighted average drag coefficient for the live tree and 3D-printed tree respectively. All the branches in the real-scale experiments can be considered to be in turbulent flow conditions, as even the smallest branches have a Reynolds number $\geq 10^3$ (see Fig. 9), hence, the weighted average drag coefficient of the canopy is expected to be around 1.

Table C.2
Weighted drag coefficient calculation for the average live tree.

Live tree							
Branch-order	Nb(units)	D(m)	L(m)	Frontal area(m^2)	Weight	C_D	C_{DW}
Class 1							
3 (Primary branch)	3	0.053	2.52	0.200	0.046	1.15	0.053
2	32	0.008	0.56	0.071	0.016	0.93	0.015
1	133	0.004	0.39	0.104	0.024	0.93	0.022
Class 2							
3 (Primary branch)	28	0.032	2.52	1.129	0.258	1.15	0.297
2	296	0.0051	0.56	0.422	0.096	0.93	0.090
1	1239	0.0047	0.39	1.135	0.259	0.93	0.241
Class 3							
3 (Primary branch)	57	0.01	0.82	0.234	0.053	1.15	0.061
2	239	0.0059	0.57	0.402	0.092	0.93	0.085
1	1001	0.0034	0.4	0.680	0.155	0.93	0.145
				4.38	1		1.01

Table C.3
Weighted drag coefficient calculation for the average 3D-printed tree.

Printed tree							
Branch-order	Nb(units)	D(m)	L(m)	Frontal area(m^2)	Weight	C_D	C_{Dw}
Class 1							
3 (Primary branch)	3	0.0053	0.252	0.002	0.055	1	0.055
2	24	0.001	0.056	0.001	0.019	1.58	0.029
1	48	0.001	0.039	0.001	0.026	1.58	0.041
Class 2							
3 (Primary branch)	28	0.0032	0.252	0.011	0.311	1	0.311
2	168	0.001	0.056	0.005	0.130	1.58	0.205
1	336	0.001	0.039	0.007	0.180	1.58	0.285
Class 3							
3 (Primary branch)	57	0.001	0.082	0.002	0.064	1.58	0.102
2	114	0.001	0.057	0.003	0.089	1.58	0.141
1	228	0.001	0.04	0.005	0.126	1.58	0.198
				0.04	1		1.37

The above tables show that approximately 60% of the entire frontal-surface area of the average printed willow tree is assigned to the branches with a diameter of 1 mm, the remaining branches are *order* 3 branches (i.e., largest branches) and, hence, are assigned to have a drag coefficient of 1. The weighted average drag coefficient of the canopy is around 1.37 for the printed trees.

This increase of drag coefficient (1.01 to 1.37) is approximately 37%. As the drag coefficient is linearly related to the damping ratio (β), β also increases with 37% if all the other parameters (such as A_v) are kept constant. The formula C.5 and C.6 show that for the forest width of 40 m (= constant) and wave damping of 20% (Transmission coefficient, 1–0.20 = 0.80), the damping ratio, β is around 0.00625. Increasing β by 37% (β=0.00856) leads to a transmission coefficient of 0.74, hence a wave damping ratio of 26% for the same forest in a lower Reynolds regime. As previously mentioned, a maximum 30% wave height damping was measured in the scaled experiments, and a significant amount of this can be attributed to the differences in Reynolds numbers, following the reasoning above.

C.1. Analytical formulation

The analytical solution stems from the energy balance equation:

$$\frac{\partial(Ec_g)}{\partial x} = \varepsilon_v, \tag{C.1}$$

where E is the amount of wave energy per horizontal area = $1/8\rho g H^2$; ρ = fluid density; H = wave height; c_g is the wave group velocity; ε_v = time-averaged energy dissipation rate per unit area due to vegetation. In this case the energy dissipation by vegetation will be the sum of dissipation by

every single vegetation layer, as described in Suzuki (2011).

$$\varepsilon_v = \sum_{i=1}^{I} \varepsilon_{v,i} \tag{C.2}$$

where

$$\varepsilon_{v,i} = \int_{-h+\alpha_{i-1}\cdot h}^{-h+\alpha_i \cdot h} Fu \;\; dz$$

In which F is often simplified as the drag force (namely the pressure/ or form drag force) on the plant and u is the horizontal orbital velocity. The general solution of the balance equation (first order ODE) is:

$$\frac{H_s}{H_{s,0}} = \frac{1}{1 + \frac{B_0\left(H_{s,0}/1.416\right)}{2}x} = \frac{1}{1+\beta x}, \tag{C.3}$$

where

$$\beta = \frac{1}{3\sqrt{\pi}} \frac{k_p}{sinhkh(sinh2kh + 2kh)} \left[\sum_{i=1}^{I} C_{D,i} N_i b_{v,i} \left(sinh^3 k_p \alpha_{i-1} h - sinh^3 k_p \alpha_i h\right) + 3\left(sinhk_p \alpha_{i-1} h - sinhk_p \alpha_i h\right) \right] \left(\frac{H_{s,0}}{1.416}\right),$$

where $N_i b_{v,i}$ can be written as one parameter, called the frontal surface area of vegetation in layer i, $A_{v,i}$. This β from Eq. C.3 accounts for wave energy dissipation by vegetation and the flume walls, therefore now referred to as $\beta_{veg\&flume}$. However, we need to remove bottom friction and wall friction effects and find β_{veg}. For this, we use the calibration tests (i.e., tests without vegetation). From the calibration tests we find β_{flume}. This is according to the study of Maza et al. (2019).

$$\frac{1}{1+\beta_{veg}x} = \frac{1}{1+\beta_{veg\&flume}x} - \frac{1}{1+\beta_{flume}x}, \tag{C.4}$$

where

$$\frac{H_{m0,veg}}{H_{m0,veg,in}} = \frac{1}{1+\beta_{veg\&flume}x}$$

and

$$\frac{H_{m0,no\,veg}}{H_{m0,no\,veg,in}} = \frac{1}{1+\beta_{flume}x}$$

For simplicity, we assume a one layer schematization of the forest, with constant frontal-surface area along the height as we showed that the frontal-surface area between the two scales was similar – the only vegetation parameter that varies is the drag coefficient (C_D). The definition used in this work for wave damping was according to van Wesenbeeck et al. (2022):

$$Dr = \frac{H_{m0,no\,veg} - H_{m0,veg}}{H_{m0,in}}, \tag{C.5}$$

This is equivalent to:

$$\frac{H_{m0,no\,veg} - H_{m0,veg}}{H_{m0,in}} = 1 - \frac{1}{1+\beta_{veg}x} \tag{C.6}$$

Thus, an increase of 10 percentage points of Dr will lead to a decrease of 10 percentage points of $\frac{1}{1+\beta_{veg}x}$.

References

Achenbach, E., 1968. Distribution of local pressure and skin friction around a circular cylinder in cross-flow up to Re = 5:106. J. Fluid Mech. 34, 625–639. https://doi.org/10.1017/S0022112068002120.

Armanini, A., Righetti, M., Grisenti, P., 2005. Direct measurement of vegetation resistance in prototype scale. J. Hydraul. Res. 43, 481–487. https://doi.org/10.1080/00221680509500146.

Bao, T.Q., 2011. Effect of mangrove forest structures on wave attenuation in coastal Vietnam. Oceanologia 53, 807–818. https://doi.org/10.5697/oc.53-3.807.

Cavallaro, L., Viviano, A., Paratore, G., Foti, E., 2018. Experiments on Surface Waves Interacting with Flexible Aquatic Vegetation, vol. 53. https://doi.org/10.1007/s12601-018-0037-8.

Dalrymple, R.A., Kirby, J.T., Hwang, P.A., 1984. Wave diffraction due to areas of energy dissipation. J. Waterw. Port Coast. Ocean Eng. 110, 67–79. https://doi.org/10.1061/(ASCE)0733-950X(1984)110:1(67).

He, F., Chen, J., Jiang, C., 2019. Surface wave attenuation by vegetation with the stem, root and canopy. Coast. Eng. 152, 103509. https://doi.org/10.1016/j.coastaleng.2019.103509.

Heller, V., 2011. Scale effects in physical hydraulic engineering models. J. Hydraul. Res. 49, 293–306. https://doi.org/10.1080/00221686.2011.578914.

Heller, V., 2017. Self-similarity and Reynolds number invariance in Froude modelling. J. Hydraul. Res. 55, 293–309. https://doi.org/10.1080/00221686.2016.1250832.

Hu, Z., Suzuki, T., Zitman, T., Uittewaal, W., Stive, M., 2014. Laboratory study on wave dissipation by vegetation in combined current-wave flow. Coast. Eng. 88, 131–142. https://doi.org/10.1016/j.coastaleng.2014.02.009.

Hughes, S.A., 1993. Laboratory wave reflection analysis using co-located gages. Coast. Eng. 20, 223–247. https://doi.org/10.1016/0378-3839(93)90003-Q.

Infantes, E., Orfila, A., Simarro, G., Terrados, J., Luhar, M., Nepf, H., 2012. Effect of a seagrass (Posidonia oceanica) meadow on wave propagation. Mar. Ecol. Prog. Ser. 456, 63–72. https://doi.org/10.3354/meps09754.

IPCC, 2022. Synthesis report - climate change 2023. In: An Assessment of the Intergovernmental Panel on Climate Change, 335, p. 1318.

Ismail, H., Abd Wahab, A.K., Alias, N.E., 2012. Determination of mangrove forest performance in reducing tsunami run-up using physical models. Nat. Hazards 63, 939–963. https://doi.org/10.1007/s11069-012-0200-y.

Jacobsen, N.G., Bakker, W., Uijttewaal, W.S., Uittenbogaard, R., 2019. Experimental investigation of the wave-induced motion of and force distribution along a flexible stem. J. Fluid Mech. 1036–1069 https://doi.org/10.1017/jfm.2019.739.

Kalloe, S.A., Hofland, B., Antolínez, J.A., van Wesenbeeck, B.K., 2022a. a. Quantifying Frontal-Surface Area of Woody Vegetation: a crucial Parameter for Wave Attenuation. Front. Mar. Sci. 9, 1–18. https://doi.org/10.3389/fmars.2022.820846.

Kalloe, S.A., Hofland, B., van Wesenbeeck, B.K., 2022b. Development of Scaled Tree Mimics for Wave Damping, in: 39th IAHR World Congress, Granada, Spain, pp. 2618–2625. https://www.iahr.org/library/infor?pid=21047. https://doi.org/10.3850/IAHR-39WC2521711920221137.

Kelty, K., Tomiczek, T., Cox, D.T., Lomonaco, P., Mitchell, W., 2022. Prototype-Scale Physical Model of Wave Attenuation through a Mangrove Forest of Moderate Cross-Shore Thickness: LiDAR-Based Characterization and Reynolds Scaling for Engineering with Nature. Front. Mar. Sci. 8, 1–18. https://doi.org/10.3389/fmars.2021.780946.

Keulegan, G., Carpenter, L., 1958. Forces on Cylinders and Plates in an Oscillating Fluid. American Society of Mechanical Engineers (Paper 60).

Lei, J., Nepf, H., 2021. Evolution of flow velocity from the leading edge of 2-D and 3-D submerged canopies. J. Fluid Mech. 916, 1–27. https://doi.org/10.1017/jfm.2021.197.

Luhar, M., Nepf, H.M., 2016. Wave-induced dynamics of flexible blades. J. Fluids Struct. 61, 20–41. https://doi.org/10.1016/j.jfluidstructs.2015.11.007.

Mansard, E., Funke, E., 1980. The Measurement of Incident and Reflected Spectra Using a Least Squares Method, Chapter 8, pp. 154–172.

Maza, M., Lara, J.L., Losada, I.J., Ondiviela, B., Trinogga, J., Bouma, T.J., 2015. Large-scale 3-D experiments of wave and current interaction with real vegetation. Part 2: Experimental analysis. Coast. Eng. 106, 73–86. URL: doi: https://doi.org/10.1016/j.coastaleng.2015.09.010.

Maza, M., Lara, J.L., Losada, I.J., 2019. Experimental analysis of wave attenuation and drag forces in a realistic fringe Rhizophora mangrove forest. Adv. Water Resour. 131, 103376 https://doi.org/10.1016/j.advwatres.2019.07.006.

Mendez, F.J., Losada, I.J., 2004. An empirical model to estimate the propagation of random breaking and nonbreaking waves over vegetation fields. Coast. Eng. 51, 103–118. https://doi.org/10.1016/j.coastaleng.2003.11.003.

Möller, I., Kudella, M., Rupprecht, F., Spencer, T., Paul, M., Van Wesenbeeck, B.K., Wolters, G., Jensen, K., Bouma, T.J., Miranda-Lange, M., Schimmels, S., 2014. Wave attenuation over coastal salt marshes under storm surge conditions. Nat. Geosci. 7, 727–731. https://doi.org/10.1038/NGEO2251.

Mullarney, J.C., Henderson, S.M., 2010. Wave-forced motion of submerged single-stem vegetation. J. Geophys. Res. Oceans 115, 1–14. https://doi.org/10.1029/2010JC006448.

National Research Council (U.S.), 1999. Review of the Need for a Large-Scale Test Facility for Research on the Effects of Extreme Winds on Structures. National Academy Press.

Norris, B.K., Mullarney, J.C., Bryan, K.R., Henderson, S.M., 2017. The effect of pneumatophore density on turbulence: a field study in a Sonneratia-dominated mangrove forest, Vietnam. Cont. Shelf Res. 147, 114–127. https://doi.org/10.1016/j.csr.2017.06.002.

Ozeren, Y., Wren, D.G., Wu, W., 2014. Experimental investigation of wave attenuation through model and live vegetation. J. Waterw. Port Coast. Ocean Eng. 140, 1–12. https://doi.org/10.1061/(ASCE)WW.1943-5460.0000251.

Phuoc, V.L.H., Massel, S.R., 2006. Experiments on wave motion and suspended sediment concentration at Nang Hai, Can Gio mangrove forest, Southern Vietnam. Oceanologia 48, 23–40.

Quartel, S., Kroon, A., Augustinus, P.G., Van Santen, P., Tri, N.H., 2007. Wave attenuation in coastal mangroves in the Red River Delta, Vietnam. J. Asian Earth Sci. 29, 576–584. https://doi.org/10.1016/j.jseaes.2006.05.008.

Riis, T., Kelly-Quinn, M., Aguiar, F.C., Manolaki, P., Bruno, D., Bejarano, M.D., Clerici, N., Fernandes, M.R., Franco, J.C., Pettit, N., Portela, A.P., Tammeorg, O., Tammeorg, P., Rodríguez-González, P.M., Dufour, S., 2020. Global overview of ecosystem services provided by riparian vegetation. BioScience 70, 501–514. https://doi.org/10.1093/biosci/biaa041.

Sonnenwald, F., Stovin, V., Guymer, I., 2019. Estimating drag coefficient for arrays of rigid cylinders representing emergent vegetation. https://doi.org/10.1080/00221686.2018.1494050.

Starrenburg, C.V., Ijzerloo, L.V., Wal, D.V.D., Bouma, T.J., 2023. Can willows help protect? Mechnical properties of willow species for flood defense. Manuscript submitted for publication. Department of Estuarine and Delta Systems, NIOZ Royal Netherlands Institute for Sea Research.

Sumer, B., Fredsoe, J., 1998. Hydrodynamics Around Cylindrical Structures. vol. 26. World Scientific Publishing Co. Pte. Ltd., Singapore. URL: https://app-knovel-com.tudelft.idm.oclc.org/web/view/khtml/show.v/rcid:kpASOEVHC1/cid:kt006MB8S3/viewerType:khtml//root_slug:advanced-series-ocean-2/url_slug:flow-around-cylinder?b-toc-cid=kpASOEVHC1b-toc-root-slug=advanced-series-ocean-2b-toc-title=Adv, doi: https://doi.org/10.1016/S0378-3839(97)00031-8.

Sutili, F.J., Denardi, L., Durlo, M.A., Rauch, H.P., Weissteiner, C., 2010. Flexural behaviour of selected plants under static load. Hydrol. Earth Syst. Sci. Discuss. 7, 1459–1483. https://doi.org/10.5194/hessd-7-1459-2010.

Suzuki, T., 2011. Wave Dissipation over Vegetation Fields. Ph.D. thesis.. Delft University of Technology.

Tinoco, R.O., Coco, G., 2018. Turbulence as the main driver of resuspension in oscillatory flow through vegetation. J. Geophys. Res. Earth 123, 891–904. https://doi.org/10.1002/2017JF004504.

Tomiczek, T., Wargula, A., Lomónaco, P., Goodwin, S., Cox, D., Kennedy, A., Lynett, P., 2020. Physical model investigation of mid-scale mangrove effects on flow hydrodynamics and pressures and loads in the built environment. Coast. Eng. 162 https://doi.org/10.1016/j.coastaleng.2020.103791.

van Veelen, T.J., Fairchild, T.P., Reeve, D.E., Karunarathna, H., 2020. Experimental study on vegetation flexibility as control parameter for wave damping and velocity structure. Coast. Eng. 157, 103648. https://doi.org/10.1016/j.coastaleng.2020.103648.

van Wesenbeeck, B.K., Wolters, G., Antolínez, J.A.A., Kalloe, S.A., Hofland, B., de Boer, W.P., Çete, C., Bouma, T.J., 2022. Wave attenuation through forests under extreme conditions. Sci. Rep. 12, 1–8. https://doi.org/10.1038/s41598-022-05753-3. URL https://www.nature.com/articles/s41598-022-05753-3.

Vuik, V., 2019. Building Safety with Nature Salt marshes for flood risk reduction. Ph.D. thesis. Delft. doi: https://doi.org/10.4233/uuid:9339474c-3c48-437f-8aa5-4b908368c17e.

Wu, W.C., Cox, D.T., 2015. Effects of wave steepness and relative water depth on wave attenuation by emergent vegetation. Estuar. Coast. Shelf Sci. 164, 443–450. https://doi.org/10.1016/j.ecss.2015.08.009.